Electronic Supplementary Material (ESI) for Journal of Materials Chemistry C.

Supporting information

The synergistic effect of lead-free quantum dots and SnO_2 in glass-ceramics for broadband white-emission

Qiqiang Huang,[a] Jiayan Liao,[*b] Qinyang Zhang,[a] Niu Lai,[a] Bowen Zhang,[a] Chong Wang,[a] Jie Yang,[a] Yu Yang,[a] Juan Wang,[a] Genlin Zhang,[a] Xiaoming Wen,[*c] Rongfei Wang,[*a]

[a]National Center for International Research on Photoelectric and Energy Materials, School of Materials and Energy, Yunnan University, Kunming 650091, China

[b]Institute for Biomedical Materials and Devices (IBMD), Faculty of Science, University of Technology Sydney, NSW 2007, Australia

[c]Centre for Translational Atomaterials, Swinburne University of Technology, Hawthorn 3122, Australia

Corresponding Author E-mail: jiayan.liao@uts.edu.au; xwen@swin.edu.au; rfwang@ynu.edu.cn.

This file includes:

Supplementary Figures S1 to S14

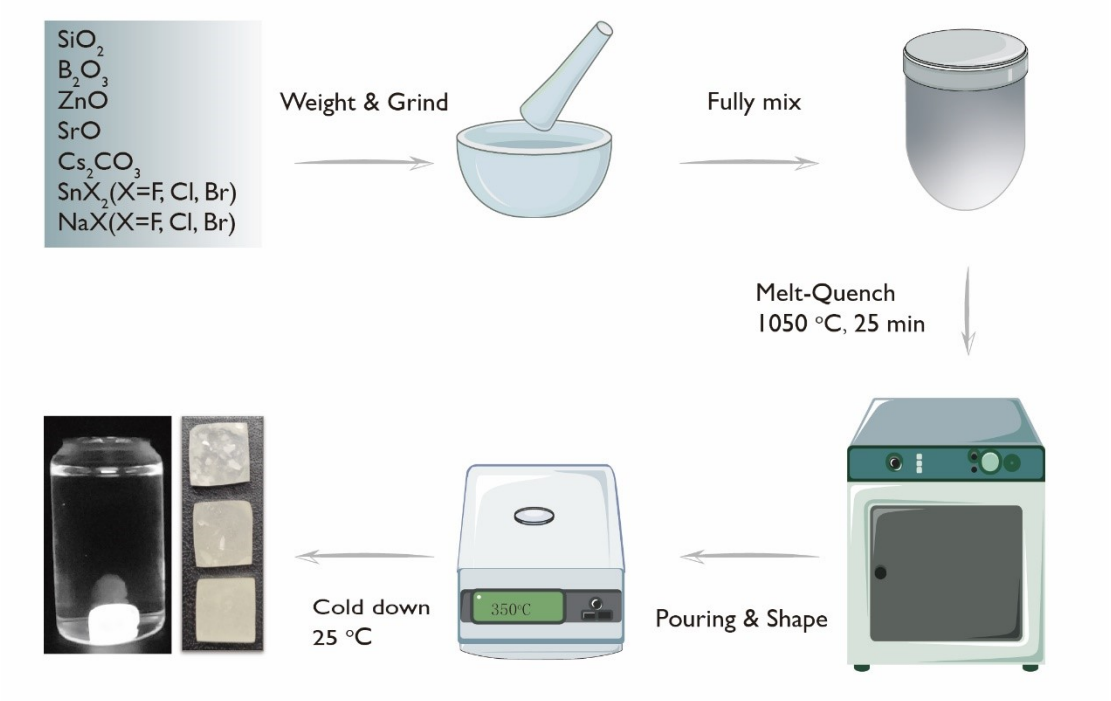

Fig. S1. Schematic diagram of the QDs glass-ceramics preparation process.

The schematic diagram of the preparation process is shown in **Fig. S1**. A certain mass of raw materials (about 10 g) is weighed according to the stoichiometric ratio and placed in a mortar to be fully ground. The mixture was poured into a corundum crucible and placed in a high-temperature furnace at 1050 °C for 25 minutes. The glass melt was then poured into a graphite mold preheated at 350 °C and cooled to room temperature naturally. The shaped QDs and SnO_2 in glass-ceramics are cut, ground and polished to obtain the above samples.

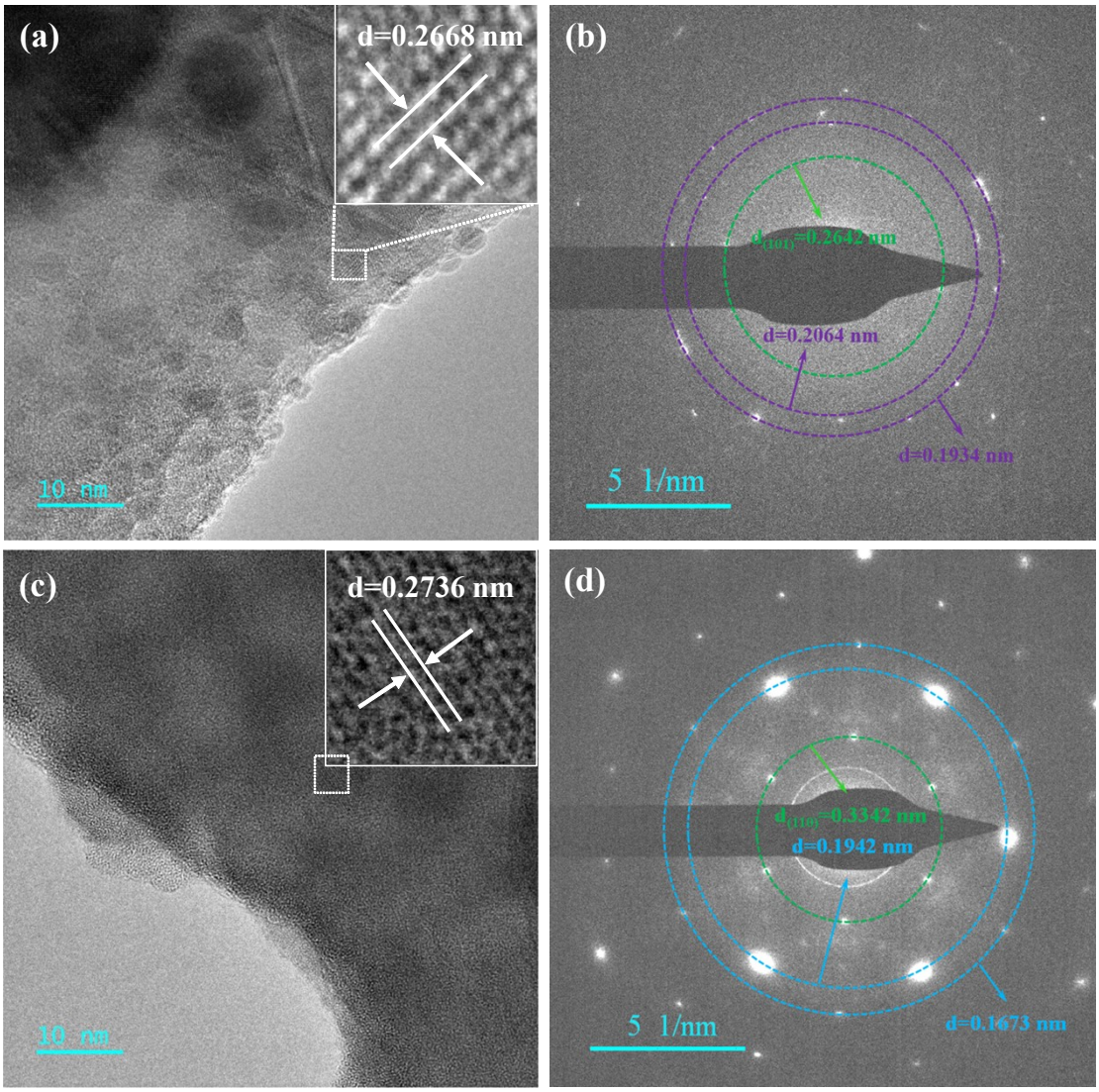

Fig. S2. (a) The TEM with crystal plane spacing of sample Sn-F. (b) the SAED pattern of sample Sn-F (purple circle: $CsSnF_3$ crystal plane, green circle: SnO_2 crystal plane). (c) The TEM with the crystal plane spacing of sample Sn-Cl. (d) SAED pattern of sample Sn-Cl (blue circle: $CsSnCl_3$ crystal plane, green circle: SnO_2 crystal plane).

Table S1 The comparison of the crystal plane spacing of the Sn-F sample and $CsSnF_3$ (PDF#00-020-0291) phase, SnO (PDF#72-2324) phase.

Sn-F Sample	**$CsSnF_3$ PDF#00-020-0291**	**SnO PDF#72-2324**
0.2668 nm	$d_{(121)}$=0.267 nm	$d_{(110)}$=0.2624 nm
0.2064 nm	$d_{(312)}$=0.205 nm	$d_{(002)}$=0.215 nm
0.1934 nm	$d_{(022)}$=0.1947 nm	$d_{(200)}$=0.191 nm

Table S2 The comparison of the crystal plane spacing of the Sn-Cl sample and $CsSnCl_3$ (PDF#74-2058) phase, SnO (PDF#72-2324) phase.

Sn-Cl Sample	$CsSnCl_3$ PDF#74-2058	SnO PDF#72-2324
0.2736 nm	$d_{(200)}$=0.2752 nm	$d_{(011)}$=0.2765 nm
0.1942 nm	$d_{(220)}$=0.1946 nm	$d_{(200)}$=0.191 nm
0.1673 nm	$d_{(311)}$=0.166 nm	$d_{(021)}$=0.1663 nm

Fig. S2 shows the TEM with crystal plane spacing and Selected Area Electron Diffraction (SAED) images of Sn-F and Sn-Cl samples. **Tables S1 and S2** summarize the comparison between the crystal plane spacing from the HR-TEM images/SAED patterns and $CsSnF_3$ (PDF#00-020-0291), $CsSnCl_3$ (PDF#74-2058), SnO (PDF#72-2324) standard crystal phase.

From **Table S1** and **Fig. S2 (a)** and **(b)**, The crystal plane spacing of sample Sn-F in **Fig. S2 (a)** is 0.2668 nm, matching well with the (121) crystal plane spacing (d=0.267 nm) of $CsSnF_3$ (PDF#00-020-0291). Compare with the (002) crystal plane (d=0.215 nm) and (200) crystal plane (d=0.191 nm) of SnO (PDF#72-2324), the spacing of the two crystal planes from the SAED pattern is 0.2064 nm and 0.1934 nm (purple circle), which match better with the (312) crystal plane (d=0.205 nm) and (022) crystal plane (d=0.1947 nm) of $CsSnF_3$. Except for the crystal planes from $CsSnF_3$, one of the crystal planes spacing (0.2642 nm) in the SAED pattern (green circle) matches well with the (101) crystal plane (d=0.26427 nm) of the main crystalline SnO_2 phase in the sample Sn-F (**Fig. S2 (b)**).

From **Table S2** and **Fig. S2 (a)** and **(b)**, The crystal plane spacing of sample Sn-Cl in **Fig. S2 (c)** is 0.2736 nm, matching well with the (200) crystal plane spacing (d=0.2752 nm) of $CsSnCl_3$ (PDF#74-2058). The spacing of the other two crystal planes from the SAED pattern is 0.1942 nm and 0.1673 nm, which match well with the (220) crystal plane (d=0.1946 nm) and (311) crystal plane (d=0.166 nm) of $CsSnCl_3$. While these two spacing are also close to the (200) crystal plane (d=0.191 nm) and (021) crystal plane (d=0.1663 nm) from SnO. A crystal plane spacing (0.3342 nm) in the SAED pattern (green circle) matches well with the (110) crystal plane (d=0.3347 nm) of the main crystalline SnO_2 phase in the sample Sn-Cl (**Fig. S2 (d)**).

The green circles represent the main SnO_2 crystal plane, the purple circles represent the $CsSnF_3$ crystal plane and the blue circles in SAED are the $CsSnCl_3$ crystal plane. There are $CsSnX_3$ (X= F, Cl, Br) QDs in these three kinds of glass-ceramics samples, and also can't exclude the existence of SnO QDs. Moreover, the SnO phase does not show the emission light, and it mainly emits light in the form of Sn^{2+} in the glass. Hence, a small amount of SnO in the samples doesn't affect the luminescence properties.[51]

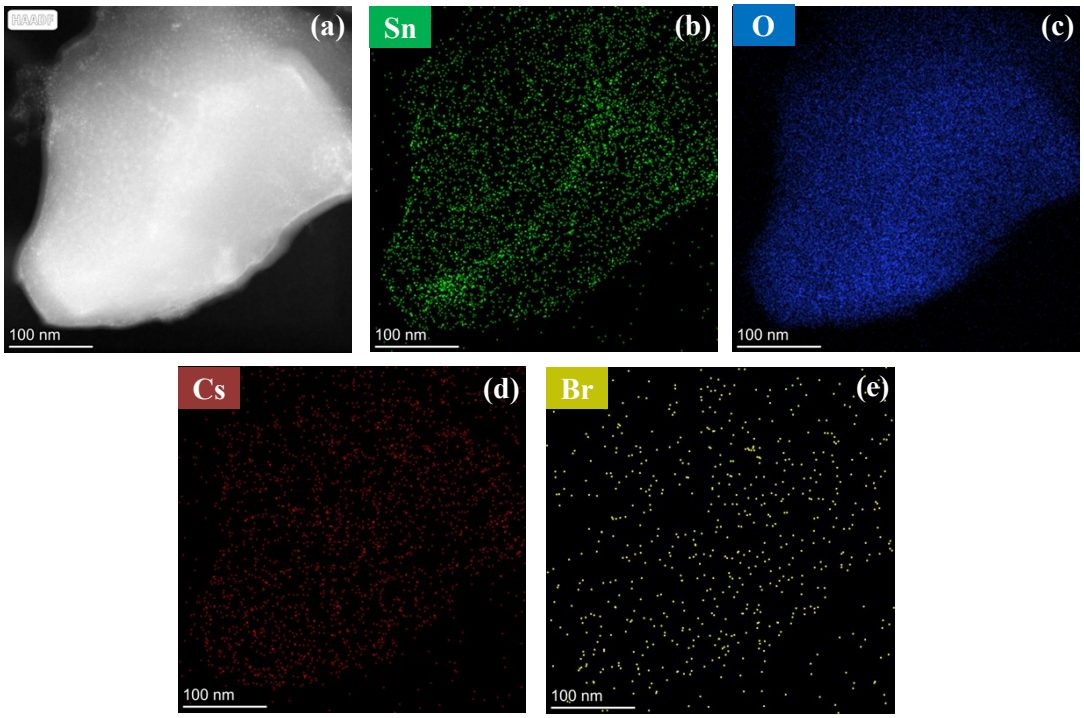

Fig. S3. (a-d) EDS mapping of Sn-Br samples with big size nanocrystals.

From the region of big size nanocrystals with strong luminescence in **Fig. S3**, there are abundant Sn and O elements, the content of Cs and Br is low, and the distribution is sparse. It indicates the large crystallite is SnO_2 nanocrystals.

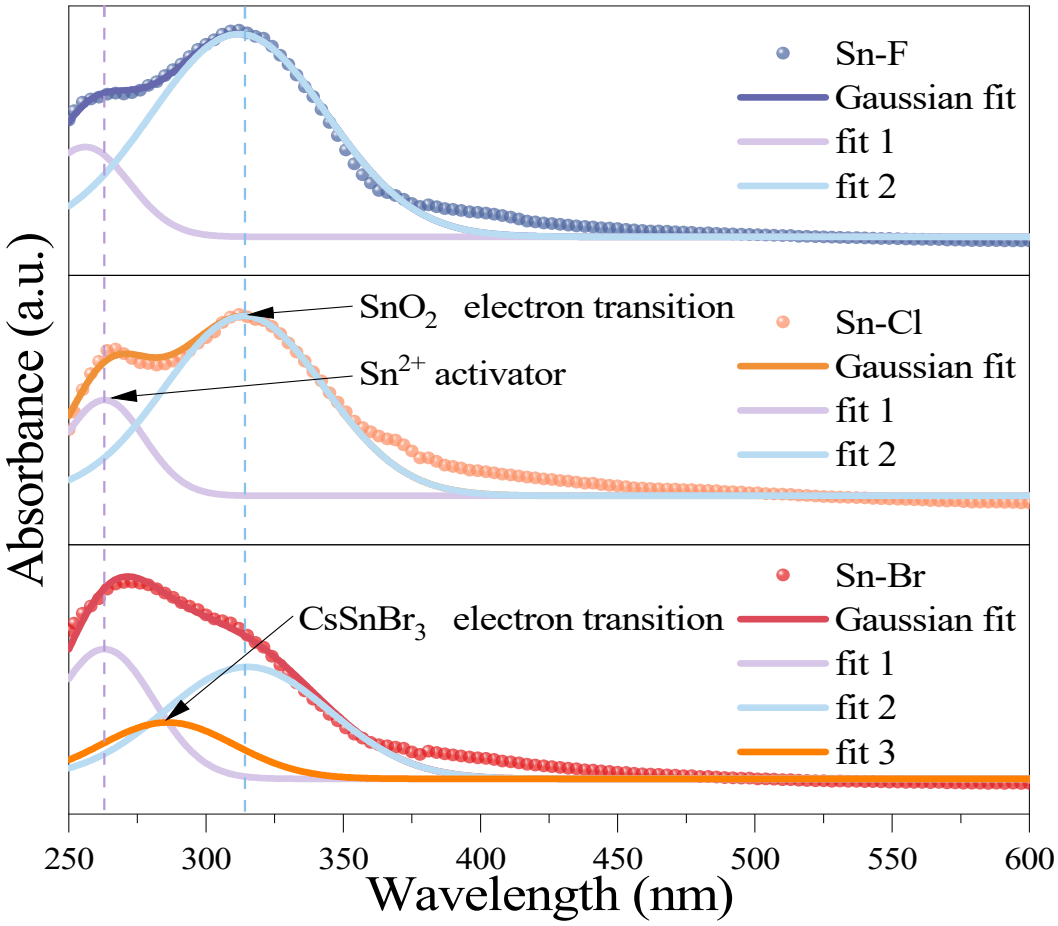

Fig. S4. Absorption spectra of Sn-F/Cl/Br samples.

Fig. S4 shows the absorption spectrum of Sn-F/Cl/Br samples, which all show broadband absorption (250-400 nm). The Sn-F and Sn-Cl samples were fitted to two peaks and the sample Sn-Br was fitted to three peaks. The three peaks after fitting were fit 1 (263 nm), fit 2 (315 nm) and fit 3 (286 nm). The absorption peak at 263 nm is mainly attributed to the Sn^{2+} activator,[S2, S3] the absorption peak at 315 nm is attributed to the direct electron transition in the SnO_2 nanocrystals,[S4] and the absorption peak at 286 nm is attributed to the electronic transition of $CsSnBr_3$ QDs.[S5] The fit 1 absorption peak in the Sn-F sample is partially offset, mainly because of the different local environments of the Sn^{2+} activator in the glass matrix.[S3]

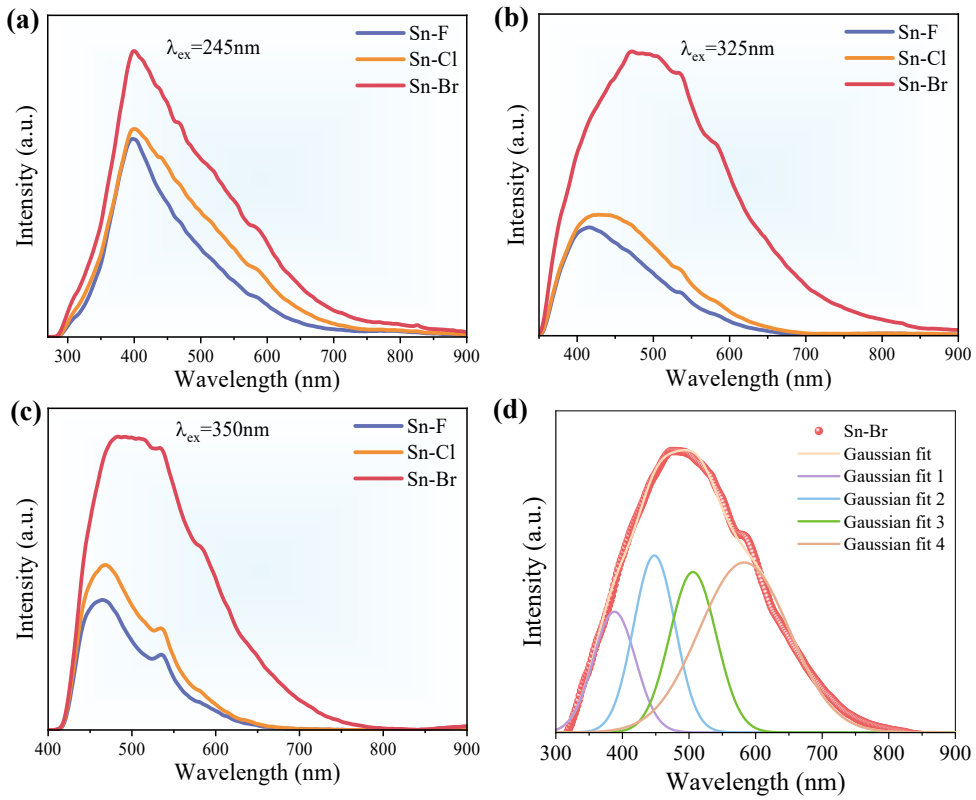

Fig. S5. (a-c) The emission spectra of the sample (Sn-F/Cl/Br) at λ_{ex}=245 nm, λ_{ex}=325 nm, and λ_{ex}=350 nm, respectively. (d) Peak fitting diagram of the emission spectrum of the sample Sn-Br.

In Fig. **S5 (a-c)**, the PL spectra of Sn-F/Cl/Br samples were measured under 245 nm, 325 nm, and 350 nm excitation, respectively and these three samples exhibit ultra-broadband emission. As the atomic radius increases from F, Cl to Br, the width of the emission spectrum broadens (e.g., 300-900 nm for Sn-Br samples) and the PL intensity increases. The most intense peak of the emission spectrum shows a red shift from Sn-F to Sn-Br samples. The Sn-Br sample shows the highest PL intensity due to the highest crystallinity, consistent with the XRD results. The peak fitting diagram of the emission spectrum of the sample Sn-Br under 289 nm excitation is shown in **Fig. S5 (d)**. Four Gaussian fitting peaks were generated after peak separation, and the peak positions were 388 nm (fit 1), 448 nm (fit 2), 506 nm (fit 3), and 583 nm (fit 4). The peaks of fit 1 can be attributed to the emission of shallow donor V_o^o defects,[S6, S7] fit 2 is from the electronic transition of $S_1 \rightarrow S_0$ of Sn^{2+}.[S2, S8] The fit 3 and fit 4 peaks are from the emission of $CsSnBr_3$ QDs[S9, S10] and SnO_2,[S4] respectively.

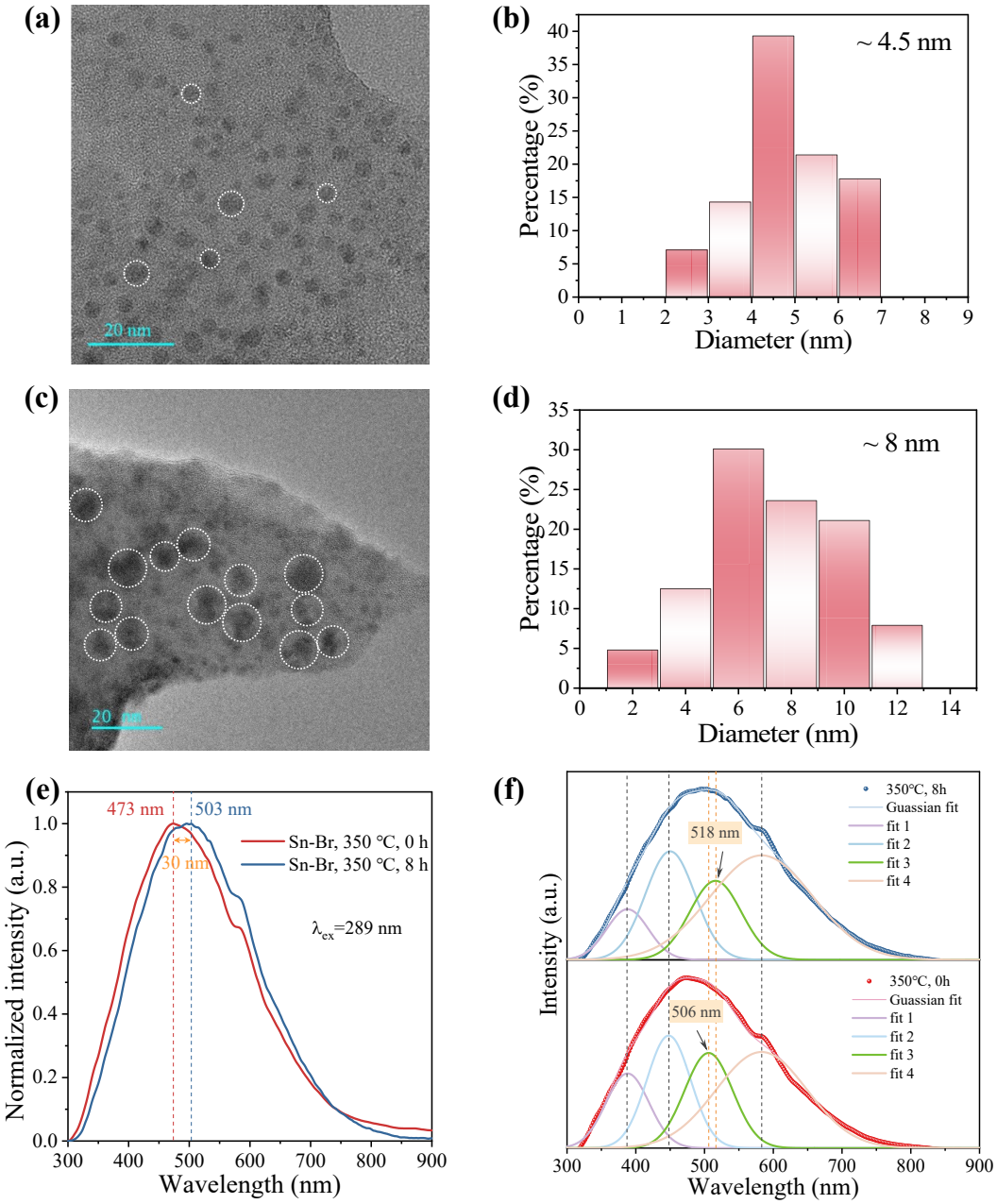

Fig. S6. (a) and (b) the TEM photo and histogram of the grain size distribution of sample Sn-Br before heat treatment. (c) and (d) the TEM image and histogram of the grain size distribution of the Sn-Br sample after heat treatment at 350 °C for 8 h. (e) Normalized emission spectra and (f) peak fitting of Sn-Br samples before and after 8 h heat treatment.

To demonstrate the quantum confinement effect of the $CsSnBr_3$ QDs, we prepared two new samples without and with heat treatment at 350 ℃ for 8 h. The HR-TEM, emission of these two samples was tested in **Fig. S6**. **Fig. S6 (a-b)** shows the TEM and particle size distribution histogram of the Sn-Br sample before heat treatment and the average particle size is around 4.5 nm. After heat treatment at 350 ℃ for 8 h, the size of the $CsSnBr_3$ QDs grew significantly, with an average particle size of 8 nm, as shown in **Fig. S6 (c-d)**. **Fig. S6 (e)** was the normalized emission spectra of sample Sn-

Br before and after heat treatment under 289 nm excitation. These two samples show ultra-wideband emission spectrum ranges from 300 to 900 nm. After heat treatment, the strongest peak of the luminescence spectrum was red shifted from 473 nm to 503 nm (30 nm shift). The emission spectra of these two samples were fitted, as shown in **Fig. S6 (f)**. Four Gaussian peaks were generated in the emission spectra, and the fitting emission peak from $CsSnBr_3$ QDs was red shifted from 506 nm to 518 nm (12 nm shift) after heat treatment.

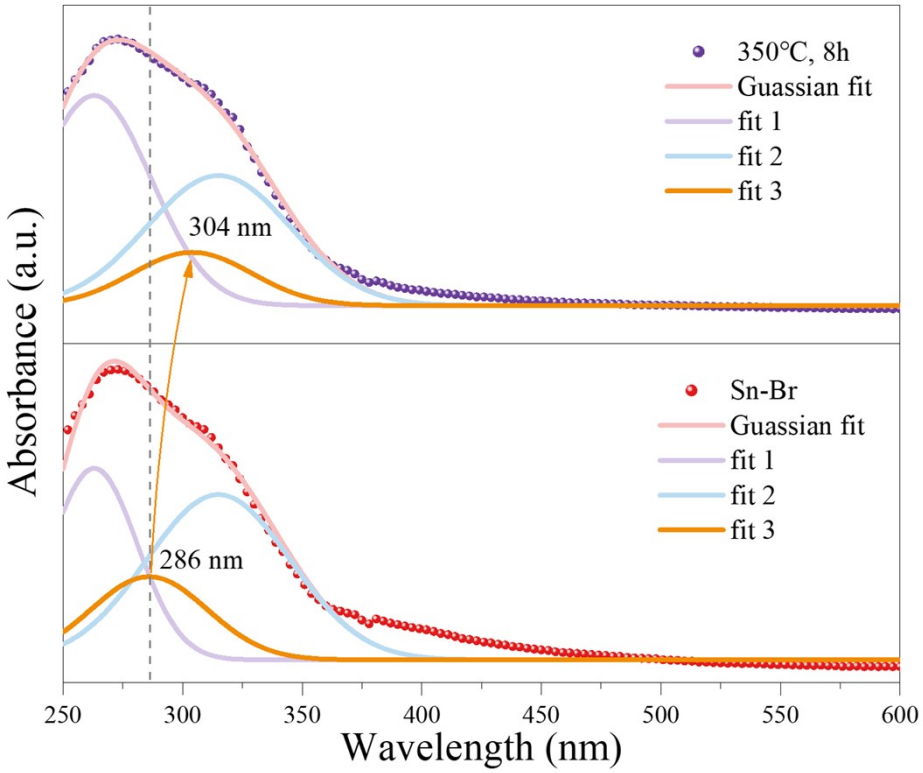

Fig. S7. Absorption spectra of sample Sn-Br before and after 8 h heat treatment.

Fig. S7 shows the absorption spectra of Sn-Br samples before and after heat treatment. After peak fitting, both samples produced three absorption peaks. The peak at fit 1 (263 nm) is mainly attributed to the absorption peak of the Sn^{2+} activator,[S2, S3] the absorption peak at fit 2 (315 nm) is attributed to the direct electron transition in SnO_2 nanocrystals,[S4] and fit 3 is attributed to the electronic transition of $CsSnBr_3$ QDs.[S5] Compared with the Sn-Br sample before heat treatment, the fit 3 absorption peak is a red shift from 286 nm to 304 nm (18 nm shift) after heat treatment. It's mainly because the heat treatment promotes the growth of $CsSnBr_3$ QDs, resulting in the red shift of the $CsSnBr_3$ absorption peak. The emission and absorption spectra of Sn-Br samples show that the spectra of $CsSnBr_3$ QDs are red-shifted after heat treatment, demonstrating the quantum confinement effect of CsSnBr QDs.

Table S3 Molar ratio of specific chemical components of G3 (**4SnBr$_2$**), G4 (**6SnBr$_2$**) and G5 (**9SnBr$_2$**) samples (total molar amount is 100).

Sample	SiO_2	B_2O_3	ZnO	SrO	Cs_2CO_3	$SnBr_2$	NaBr
G3	20	52	9	2	8	4	5
G4	20	52	9	2	8	6	3
G5	20	52	9	2	8	9	0

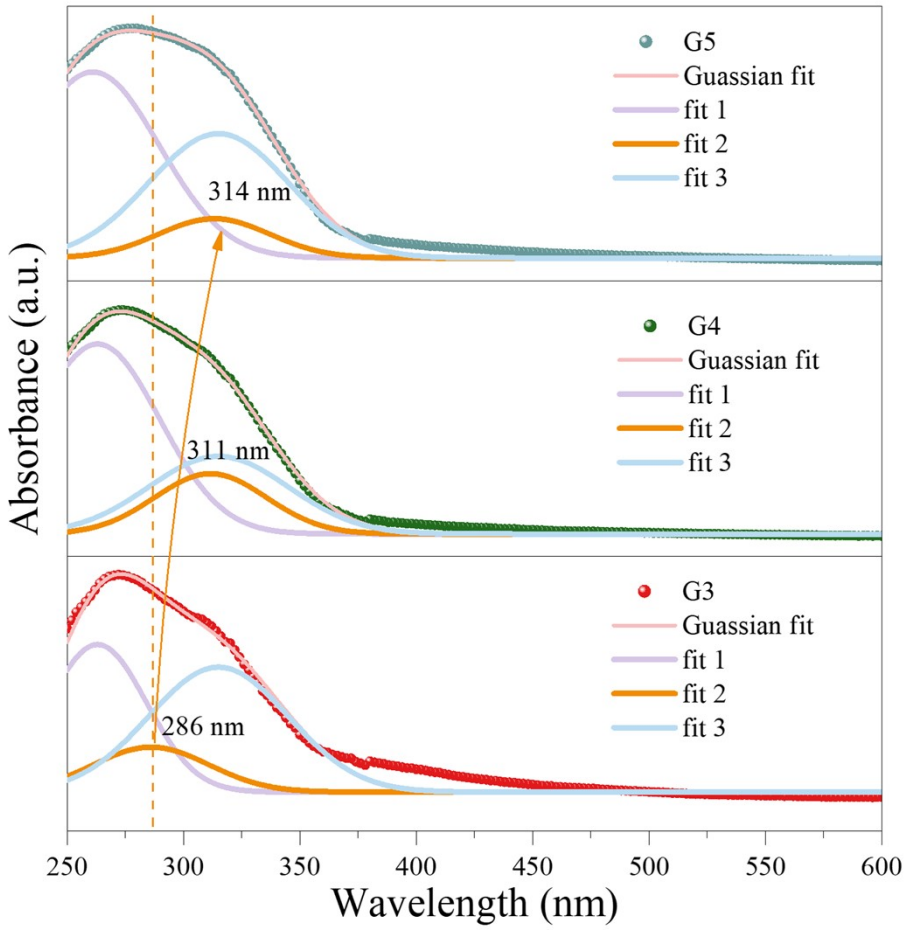

Fig. S8. Absorption spectra of different $SnBr_2$ and NaBr contents in the glass matrix. The absorption peak at 263 nm was attributed to the Sn^{2+} activator, the absorption peak at 315 nm was attributed to the direct electron transition in the SnO_2 nanocrystalline, and the absorption peak at 286 nm was attributed to the $CsSnBr_3$ electron transition.

To explore the influence of different $SnBr_2$ and NaBr contents in the glass matrix on the absorption spectra, three samples (G3, G4 and G5) were designed with increased $SnBr_2$ contents (decreased NaBr contents), as shown in **Table S3**. The absorption spectra and fitting peaks of G3-G5 samples are shown in **Fig. S8** and the three fitting peaks were fit 1 (263 nm), fit 2 (315 nm) and fit 3 (286 nm). With the increase of $SnBr_2$ content from G3 to G5 samples, the absorption peak of $CsSnBr_3$ red-shifted from 286 nm to 311 nm and 314 nm (28 nm shift). More $CsSnBr_3$ QDs were generated with the increase of $SnBr_2$ content, leading to the red-shifted absorption peak of $CsSnBr_3$ QDs.

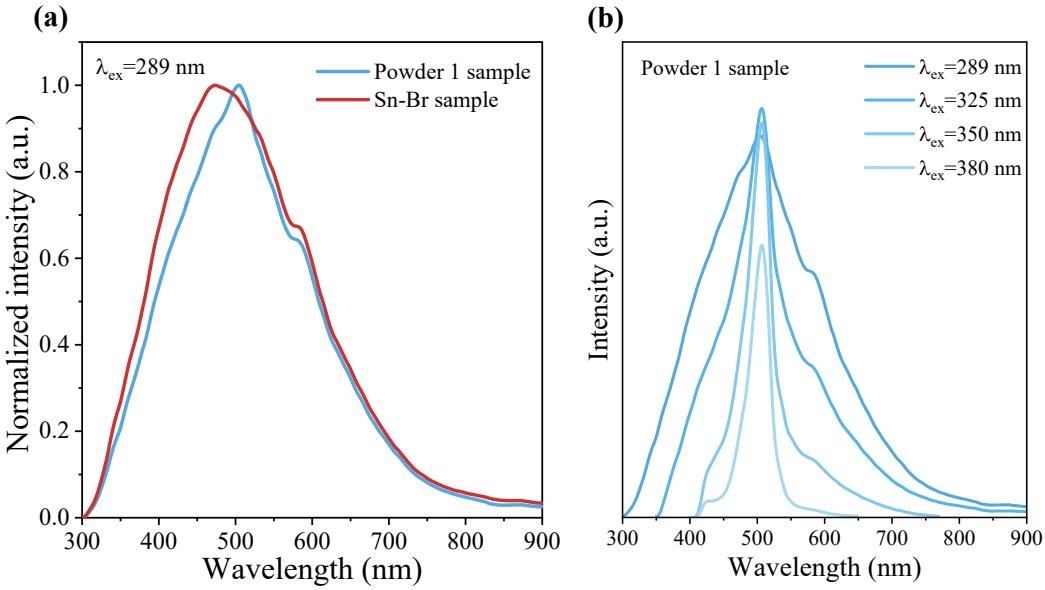

Fig. S9. (a) Emission spectra of powder 1 and fresh synthesized Sn-B sample at 289 nm. (b) Emission spectra of powder 1 at different excitation wavelengths.

The Sn-Br glass samples were cut into blocks of a certain size and ground under certain conditions for a while. After grinding, the powder is named powder 1. **Fig. S9 (a)** shows the emission spectra of powder 1 and the fresh synthesized Sn-Br samples. When the excitation wavelength is 289 nm, both powder 1 and Sn-Br samples exhibit wideband emission, but the full width at half maxima (FWHM) of powder 1 becomes narrow, and the strongest peak is red-shifted. **Fig. S9 (b)** shows the emission spectra of powder 1 at different excitation wavelengths. With the excitation wavelength increasing from 289 nm to 350 nm, the broadband emission of powder sample 1 changed to a narrow-band emission. The narrow emission peak is at 506 nm, which is consistent with emission from $CsSnBr_3$ QDs shown in previous reports.[S5, S10]

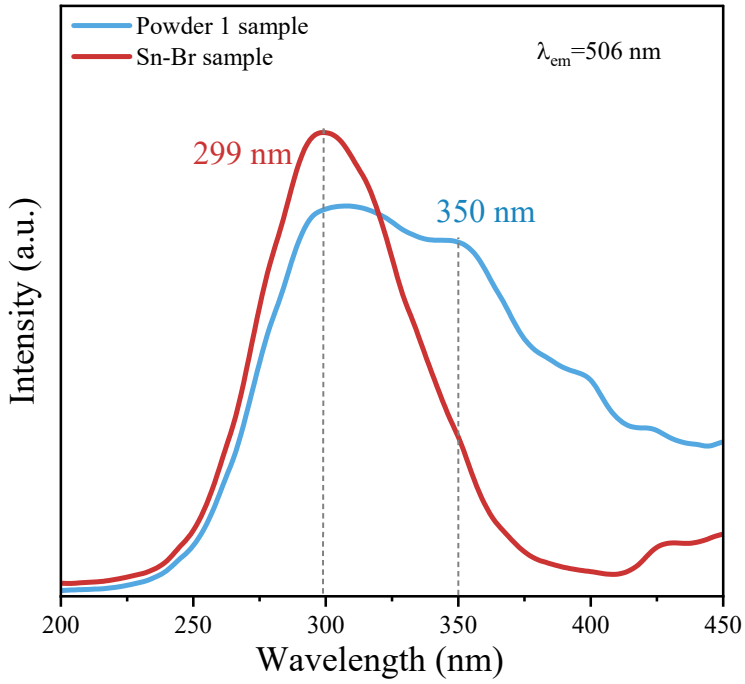

Fig. S10. Monitoring the excitation spectra of powder 1 and Sn-Br fresh sample at 506 nm.

Fig. S10 is the excitation spectrum of the powder 1 and fresh Sn-Br samples when monitoring at 506 nm. It can be seen from the figure that the excitation spectra of both powder 1 and the Sn-Br sample belong to broadband. The excitation peak at 299 nm belongs to the excitation of SnO_2,[S4] and the excitation peak at 350 nm belongs to the excitation of $CsSnBr_3$ QDs.[S11]

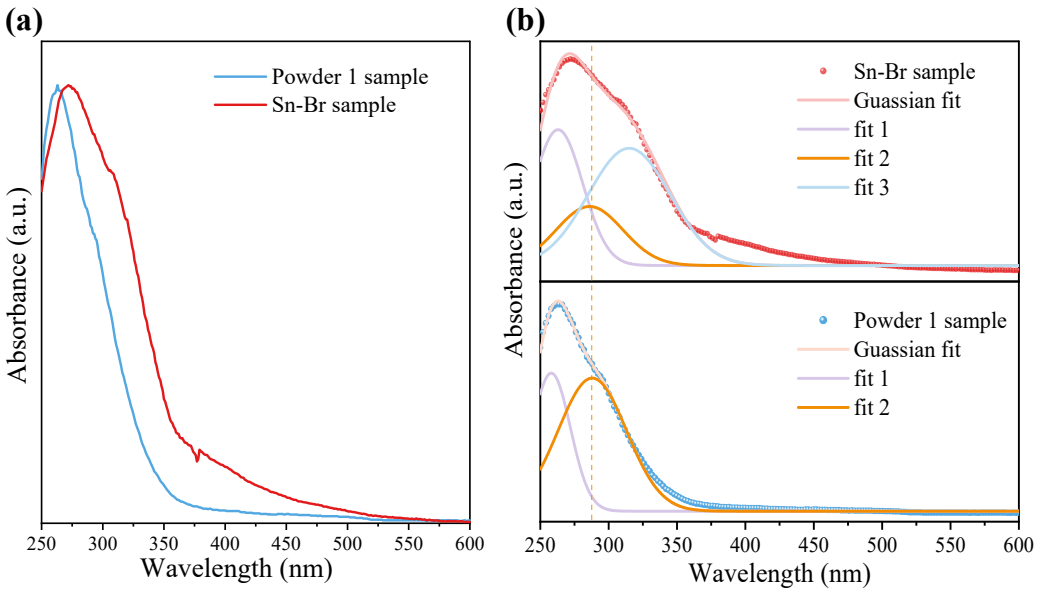

Fig. S11. (a) Absorption spectra of powder 1 sample and fresh Sn-Br sample after normalization. (b) Peak fitting diagram of absorption spectra of powder 1 and fresh Sn-Br samples.

The absorption spectra of powder 1 and the fresh synthesized Sn-Br samples were tested, as shown in **Fig. S11 (a)** and **(b)**. The powder 1 sample contains less SnO_2, resulting in a narrow absorption spectrum. The powder 1 sample contains two fitting peaks, which were fit 1 (258 nm) and fit 2 (286 nm). The fresh Sn-Br sample contains three fitting peaks: fit 1 (263 nm), fit 2 (286 nm) and fit 3 (315 nm). The fit 1 peak is attributed to the absorption peak of the Sn^{2+} activator,[S2, S3] the fit 2 peak is the electronic transition of $CsSnBr_3$ QDs,[S5] and the fit 3 peak is the direct transition of electrons in SnO_2 nanocrystals.[S4] The fit 1 absorption peak in powder 1 is slightly shifted, mainly because of the different local coordination environments of Sn^{2+} ions.[S3]

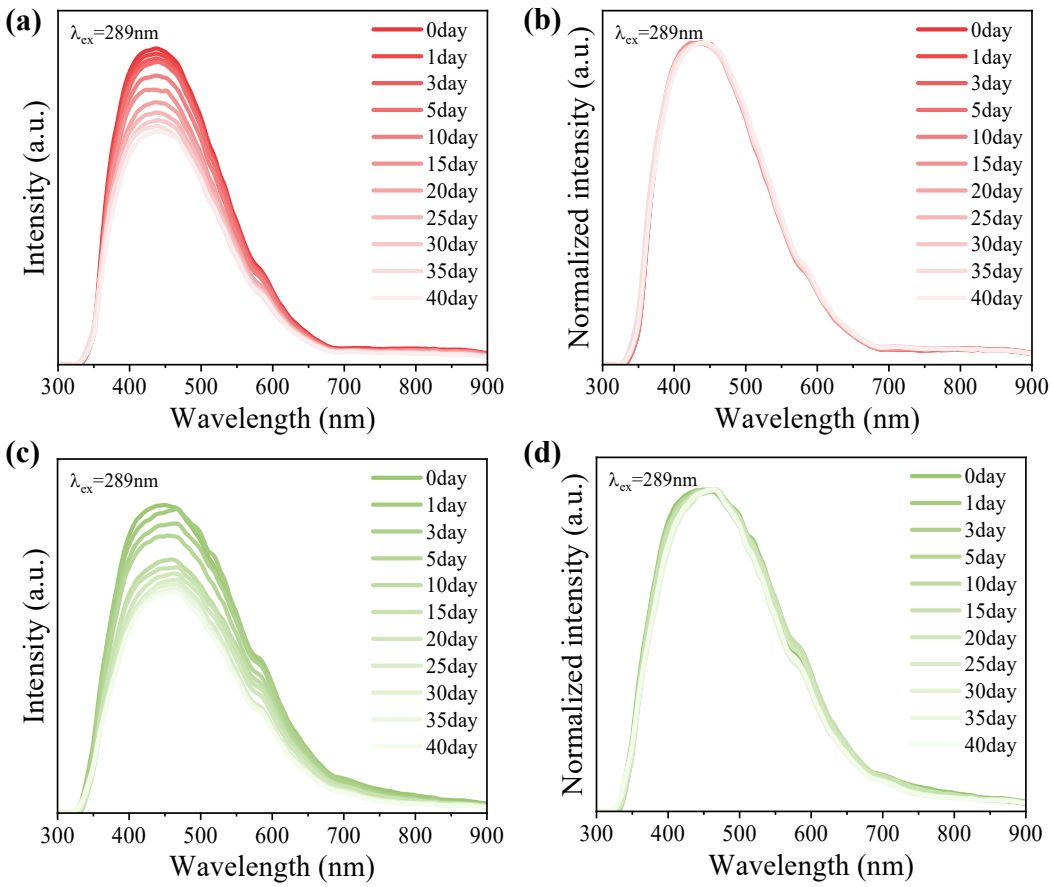

Fig. S12. (a) PL spectra of Sn-F sample immersed in water for different times up to 40 days and (b) the corresponding normalized spectra; (c) PL spectra of Sn-Cl sample immersed in water for different times up to 40 days and (d) the corresponding normalized spectra.

The luminescence intensity of Sn-F/Cl QDs glass-ceramics was periodically measured when immersed in water at room temperature. The 40-day luminescence intensity changes of Sn-F/Cl samples are shown in **Fig. S12**. **Fig. S12 (a)** is the PL spectra of Sn-F sample immersed in water for different times up to 40 days and **Fig. S12 (b)** is the corresponding normalized spectra. **Fig. S12 (c)** is the PL spectra of the Sn-Cl sample immersed in water for different times up to 40 days and **Fig. S12 (d)** is the corresponding normalized spectra. The results showed that the luminescence intensity decreased, and the peak shape changed slightly, indicating the stability of Sn-F/Cl QDs glass-ceramics.

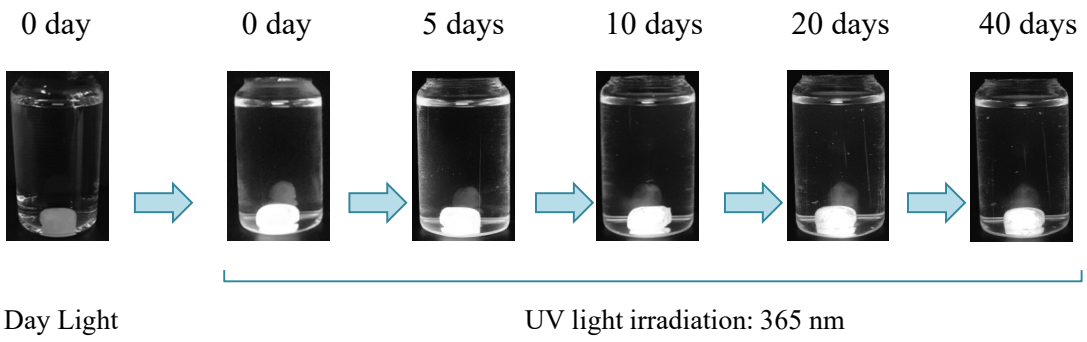

Fig. S13. The photos of the sample Sn-Br just put into water and after different times.

Fig. S13 is a photograph of the Sn-Br sample placed in water at different times, and it still maintains bright white luminescence for 40 days, which demonstrates the stability of QDs is greatly improved when encapsulated in glass.

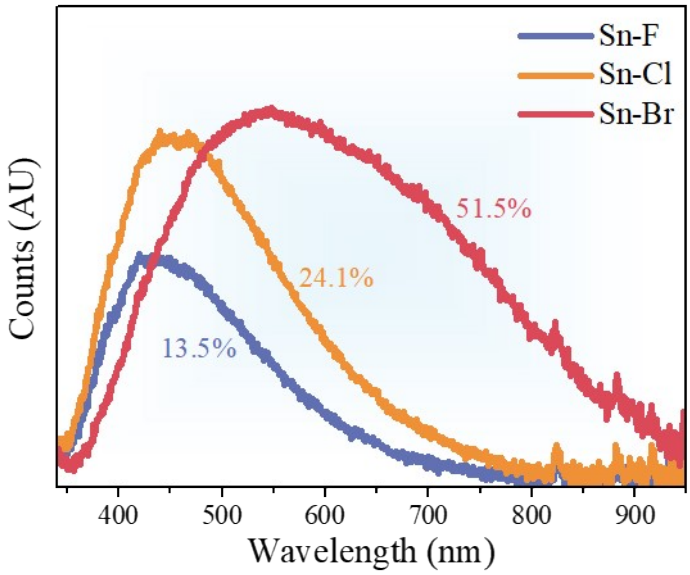

Fig. S14. Photoluminescence spectra and quantum efficiencies of the sample (Sn-F/Cl/Br).

Fig. S14 is the PLQY results of the Sn-F/Cl/Br samples, which are 13.5%, 24.1% and 51.5%, respectively.

References:

S1 W. H. Doh, W. Jeong, H. Lee, J. Park and J. Y. Park, *Nanotechnology*, 2016, **27**, 335603.

S2 H. Masai, T. Tanimoto, S. Okumura, K. Teramura, S. Matsumoto, T. Yanagida, Y. Tokuda and T. Yoko, *J. Mater. Chem. C*, 2014, **2**, 2137-2143.

S3 K. Yang, S. Zheng, X. Jiang, S. Fan and D. Chen, *Mater., Lett*. 2017, **204**, 5-7.

S4 S.-S. Chang and M. S. Jo, *Ceram. Int*., 2007, **33**, 511-514.

S5 H. Xu, J. Duan, Y. Zhao, Z. Jiao, B. He and Q. Tang, *J. Power Sources*, 2018, **399**, 76-82.

S6 V. Agrahari, M. C. Mathpal, M. Kumar and A. Agarwal, *J. Alloys Compd*., 2015, **622**, 48-53.

S7 X. Wang, X. Wang, Q. Di, H. Zhao, B. Liang and J. Yang, *Mater*., 2017, **10**, 1398.

S8 R. Wang, J. Zhang, Y. Zhang, H. Lin, E. Y.-B. Pun and D. Li, *J. Alloys Compd*., 2021, **864**, 158671.

S9 S. Liu, G. Shao, L. Ding, J. Liu, W. Xiang and X. Liang, *Chem. Eng. J*., 2019, **361**, 937-944.

S10 D. Li, W. Xu, D. Zhou, X. Ma, X. Chen, G. Pan, J. Zhu, Y. Ji, N. Ding and H. Song, *J. Lumin.*, 2019, **216**, 116711.

S11 X. Zhang, H. Wang, S. Wang, Y. Hu, X. Liu, Z. Shi, V. L. Colvin, S. Wang, W. W. Yu and Y. Zhang, *Inorg. Chem*., 2020, **59**, 533-538.